Hakimhashemi, A., Yoon, J.-S., Heidbach, O., Zang, A., Grünthal, G. (2014): Forward induced seismic hazard assessment: application to a synthetic seismicity catalogue from hydraulic stimulation modelling. - *Journal of Seismology*, *18*, 3, p. 671-680.

DOI: http://doi.org/10.1007/s10950-014-9439-y

Journal of Seismology (2014) 18: 671-680
DOI 10.1007/s10950-014-9439-y

Forward induced seismic hazard assessment: application to a synthetic seismicity catalogue from hydraulic stimulation modelling

Amir Hossein Hakimhashemi • Jeoung Seok Yoon • Oliver Heidbach • Arno Zang • Gottfried Grünthal

Received: 22 March 2013 /Accepted: 13 April 2014

Abstract The M_w 3.2-induced seismic event in 2006 due to fluid injection at the Basel geothermal site in Switzerland was the starting point for an ongoing discussion in Europe on the potential risk of hydraulic stimulation in general. In particular, further development of mitigation strategies of induced seismic events of economic concern became a hot topic in geosciences and geoengineering. Here, we present a workflow to assess the hazard of induced seismicity in terms of occurrence rate of induced seismic events. The workflow is called Forward Induced Seismic Hazard Assessment (FISHA) as it combines the results of for-ward hydromechanical-numerical models with methods of time-dependent probabilistic seismic hazard assessment. To exemplify FISHA, we use simulations of four different fluid injection types with various injection parameters, i.e. injection rate, duration and style of injection. The hydromechanical-numerical model applied in this study represents a geothermal reservoir with pre-existing fractures where a routine of viscous fluid flow in porous media is implemented from which flow and pressure driven failures of rock matrix and pre-existing fractures are simulated, and corresponding seismic moment magnitudes are computed. The resulting synthetic catalogues of induced seismicity, including event location, occurrence time and magnitude, are used to calibrate the magnitude completeness M_c and the parameters a and b of the frequency-magnitude relation. These are used to estimate the time-dependent occurrence rate of induced seismic events for each fluid injection scenario. In contrast to other mitigation strategies that rely on real-time data or already obtained catalogues, we can perform various synthetic experiments with the same initial conditions. Thus, the advantage of FISHA is that it can quantify hazard from numerical experiments and recommend a priori a stimulation type that lowers the occurrence rate of induced seismic events. The FISHA workflow is rather general and not limited to the hydro-mechanical-numerical model used in this study and can therefore be applied to other fluid injection models.

Keywords Seismic hazard • Induced seismicity • Numerical modelling • Reservoir geomechanics • Hydraulic fracturing

1. Introduction

To enhance permeability of georeservoirs, the stimulation of rock mass by means of fluid injection under high pressure is a common practice. This so-called hydraulic fracturing is well known since the fundamental paper of *Hubbert and Willis* (1957) has been applied widely. However, in the past decades, the accompanying induced seismicity became a problem not only at geothermal reservoirs but also in connection with other types of underground mining activities such as hydrocarbon exploitation, as well as potash and coal mining (*Evans et al.* 2012; *Majer et al.* 2007, 2012; *Grünthal* 2013; *Suckale* 2009, 2010). In particular, in Europe, the induced events at the geothermal site in Basel (Switzerland) related to fluid stimulation ($M_w = 3.2$ in 2006; *Häring et al.* 2008; Deichmann and Ernst 2009; *Deichmann and Giardini* 2009) and in Landau (Germany) due to a shut-in in the production phase ($M_w = 2.6$ in 2009; *Grünthal* 2013) were the nucleus of an intense and ongoing discussion since both sites are situated in the suburb of the respective cities. For the Basel geothermal site, the induced event even resulted in the termination of the whole project. We consider such events and use here the abbreviation SEECo for Seismic Events of Economic Concern following the arguments and definition of *Grünthal* (2013). The magnitude of the SEECo changes from site to site, e.g. in remote areas such

A. H. Hakimhashemi • J. S. Yoon • O. Heidbach (✉) • A. Zang • G. Grünthal
Helmholtz Centre Potsdam, GFZ German Research Centre for Geosciences, Section "Seismic Hazard and Stress Field", Telegrafenberg, 14473 Potsdam, Germany
e-mail: oliver.heidbach@gfz-potsdam.de

as Cooper Basin in Australia or in areas where the background seismicity of natural tectonic events is high, the magnitude level of SEECo is higher compared to urban areas with vulnerable infrastructure. Furthermore, the change of the occurrence rate of SEECo that is acceptable due to the man-made changes of the in situ stress state also depends on the individual regulatory framework. However, regardless of the local setting, stimulation strategies are needed that mitigate and lower the occurrence (rate) of SEECo. In particular, there is a need to provide practical recommendations which underground treatment strategy - that holds on for drilling, stimulation and long-term production at any georeservoir - has the least impact on the induced seismicity but increases the reservoir permeability sufficiently.

So far, several mitigation strategies have been suggested and partly tested in practice. *Bommer et al.* (2006) proposed a traffic light system that uses the observed seismicity in quasi real-time. The approach is designed such that when the observed peak ground acceleration reaches a certain threshold, the stimulation is stopped. This approach was also tested during the hydraulic fracturing at the geothermal site in Basel. However, it was not successful; the fluid injection was halted after the monitoring of $M_L = 2.6$ event followed by a substantial increase in the seismicity rate in general, but a few hours after this shut-in, the $M_w = 3.2$ event occurred (*Häring et al.* 2008; *Deichmann and Giardini* 2009). Furthermore, from a practical point of view, the traffic light system cannot give recommendations on how to plan the fluid injection strategy once the threshold of seismicity rate and/or peak ground acceleration is reached.

Shapiro et al. (2010) and *Dinske and Shapiro* (2013) proposed a more physics-based model to describe the induced seismicity in a reservoir. They used the observed induced seismicity of the injection phase to estimate the seismic potential of the site in order to produce a certain magnitude-frequency distribution. However, due to the model assumption that pressure according to fluid injection must be constant or monotonically increasing, their approach is not applicable to the shut-in phase or to the other types of reservoir stimulation such as cyclic stimulation. The statistical model by *Barth et al.* (2013) focuses on changes in probability of occurrence of an induced event after the shut-in. All abovementioned models have in common that they require a catalogue of monitored induced seismicity from a stimulation experiment. Therefore, they cannot deliver any strategy a priori how to better operate the reservoir in order to lower the SEECo occurrence rate.

An alternative way to the statistical treatment of monitored induced seismicity is to use computer simulations that model the thermal and/or hydromechanical coupled processes that change the stress into critical state (e.g. *Bruel* 2007; *Kohl and Megel* 2007; *Rutqvist et al.* 2007; *Altmann et al.* 2010; *Baisch et al.* 2010; *Schoenball et al.* 2010; McClure and Horne 2011). In most cases, the model outputs are spatiotemporal changes of rock stress and fluid pressure. Only a few hydromechanical-numerical models have the capability of producing synthetic catalogues of induced seismicity either due to preexisting faults (*Bruel* 2007) or on both, preexisting faults as well as new fractures of intact rock (*Yoon et al.* 2013, 2014). These models have in common that they can deliver a priori recommendations on how to perform the fluid injection in order to enhance permeability to a level of economic production for geothermal sites. At the same time, the permeability enhancement is expected to accompany lowered occurrence rate of SEECo (*Zang et al.* 2013).

However, the translation of the results of hydromechanical-numerical models into occurrence rate of SEECo is not established. Thus, we propose in this paper a general workflow that links the results of hydromechanical-numerical models to time-dependent probabilistic seismic hazard assessment in terms of the occurrence rate of SEECo. The estimation of the occurrence rate of SEECo is an independent method for measuring the effectiveness of the mitigation strategy and comes from a probabilistic-statistical model. The quality of the results depends mainly on the reliability of the synthetic catalogue generated by the hydromechanical-numerical model. Thus, we here propose combining both in a workflow.

This workflow is named Forward Induced Seismic Hazard Assessment (FISHA) in order to emphasize that this approach has predictive power (Fig. 1). To exemplify the workflow, we use the results of *Yoon et al.* (2013, 2014) where various types of fluid injection are tested, and seismicity catalogues are obtained. We present the results of the FISHA workflow where the synthetic catalogues of induced seismicity, including event location, time and magnitude, are used to calibrate the magnitude completeness (M_c), the frequency-magnitude relation (*Gutenberg and Richter* 1956), the time-dependent *a* and *b* parameters and the seismicity rate for each scenario in different time intervals. Using these parameters, the time-dependent occurrence rate of SEECo is calculated. These results can be used for choosing a stimulation strategy that poses the largest mitigation effect of the induced seismicity, in particular the SEECo, to be applied to a given site.

2. FISHA - forward induced seismic hazard assessment

The FISHA workflow has two branches representing the two classes of geomechanical-numerical models (Fig. 1). The right branch is related to the majority of models that

deliver only spatiotemporal stress changes. Here, the stress change can be translated into time-dependent seismicity rate, i.e. *a* values of the frequency-magnitude relation, using the rate-and-state law of *Dieterich* (1994). Details and an example of this FISHA workflow branch are presented by *Hakimhashemi et al.* (2014).

The left branch of FISHA is the focus of this paper. Here, hydromechanical-numerical models can be incorporated that are capable of simulating induced seismic events including occurrence time, location and magnitude, resulting in a synthetic catalogue of induced seismicity. The statistical seismic hazard model, i.e. the model to estimate the SEECo occurrence rate using the synthetic seismic catalogues, is based on the frequency-magnitude relation with time-dependent parameters of *a* and *b*.

In the following two sections, we briefly describe the hydromechanical-numerical model that generates a synthetic catalogue of induced seismicity for the FISHA testing and the seismic hazard model. More details of the technical background of the hydromechanical numerical model are given in *Yoon et al.* (2013, 2014) and *Zang et al.* (2013).

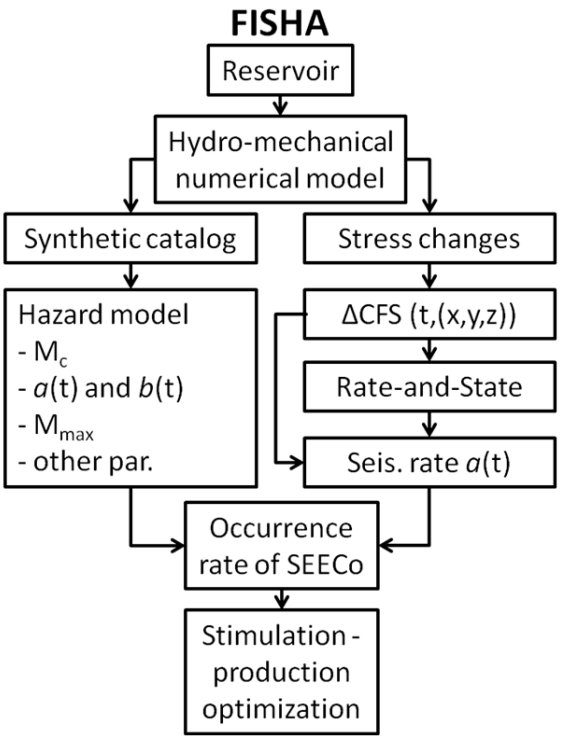

Figure 1. Structure of the Forward Induced Seismic Hazard Assessment (FISHA) workflow, divided into two branches corresponding to the output of the hydromechanical-numerical model, one based on synthetic catalogues (*left*) and the other based on Coulomb Failure Stress changes (*right*). ΔCFS (t (x, y, z)) refers to spatiotemporal changes in Coulomb Failure Stress. M_c is the magnitude completeness, a(t) and b(t) are time-dependent parameters of the frequency-magnitude relation, M_{max} is the maximum possible magnitude and SEECo are Seismic Events of Economic Concern.

3. Discrete element fracture network model

The geothermal reservoir is represented by a discrete element fracture network model using the Itasca PFC2D© code with additionally implemented hydromechanical coupled routine (*Yoon et al.* 2013, 2014). The latter enables us to model the flow of a viscous fluid in porous media. Flow-driven failure of rock matrix and pre-existing fractures are simulated in two types: mode I (tensile) and mode II (shear). Upon failure of both rock matrix and pre-existing discrete fractures, stored strain energy is released and propagates as a seismic wave. The implemented seismicity-computing algorithm (*Yoon et al.* 2013, 2014) which is modified from *Hazzard and Young* (2002, 2004) computes moment tensors of the mode I and II failures from which seismic moment (M_0) and moment magnitude (M_w) are computed.

Figure 2 shows the 2D discrete element fracture network model representing a crystalline geothermal reservoir with pre-existing fractures. For intact rock matrix, strength and deformation attributes are assigned to resemble the crystalline rock mass of Soultz-sous-Forêts, France. Mechanical and hydromechanical coupled parameters for the discrete fractures are also taken from a crystalline environment from the Forsmark site, Sweden. The modelling parameters can be found in *Yoon et al.* (2014), their table 1 and in more detail in *Zang et al.* (2013), in supplementary material. The model is calibrated against Soultz granite properties, but not validated against observed seismicity catalogue because of 2D nature of the model. Failure of rock matrix and pre-existing fractures is governed by the Mohr-Coulomb criterion (*Labuz and Zang* 2012).

The constructed model is 2 km × 2 km in size and subjected to compressive in situ stresses with S_H = 75 MPa and S_h = 60 MPa. The applied boundary stresses as maximum and minimum horizontal stresses (S_H, S_h) are taken from the stress-depth relation of Soultz site (*Cornet et al.* 2007, their Eq. 1a and b) at 4,000-m depth. At the injection point at the centre of the model, we test different injection scenarios. The outputs of the model are distribution of fluid pressure in space and time and catalogues of the induced seismic events, with occurrence time, location and magnitude. The injection is controlled by the flow rate in l/s over time. Details on the injection scenarios are given in the section where the results of the FISHA workflow are presented.

4. Hazard model

In order to calculate the SEECo occurrence rate, the parameters of the frequency-magnitude relation (*Gutenberg and Richter* 1956), i.e. *a* and *b* values, are estimated for

each injection scenario. The frequency-magnitude relation explains the exponential distribution of earthquake magnitudes in a given region as:

$$\log N = a - b(M - M_c), \quad M \geq M_c \quad , \tag{1}$$

where N is the number of events of magnitude M, M_c is the magnitude completeness that demonstrates from which magnitude almost all events are included in a catalogue and a as well as b are the model parameters.

According to Eq. 1, the statistical distribution of the magnitudes will follow an exponential distribution with density function as

$$f(m) = \begin{Bmatrix} 0 & m < M_c \\ \beta e^{-\beta(m-M_c)} & m \geq M_c \end{Bmatrix}, \tag{2}$$

where $\beta = b \cdot \ln 10$. If a maximum magnitude (M_{max}) is given, Eq. 2 will be changed to

$$f(m) = \begin{Bmatrix} \dfrac{\beta e^{-\beta(m-M_c)}}{1 - e^{-\beta(M_{max}-M_c)}} & M_c \leq m \leq M_{max} \\ 0 & otherwise \end{Bmatrix}. \tag{3}$$

Since the synthetic catalogues of induced seismicity are not complete, a maximum likelihood estimator (*Stigler* 2007) will be first applied to calculate M_c for each individual synthetic catalogue. For each catalogue, M_c can be estimated, considering a potential set of possible M_c, given an M_{max}. Then, for each possible M_c, the corresponding logarithmic likelihood function of the free parameter β, i.e. $l(\beta)$, can be written as

$$l(\beta) = \ln\left(\prod_{m \in M} f(m)\right) = \sum_{m \in M} \ln\left(\frac{\beta e^{-\beta(m-M_c)}}{1 - e^{-\beta(M_{max}-M_c)}}\right), \tag{4}$$

where M is the set of magnitudes $\geq M_c$. Then $\hat{\beta}$, i.e. the estimation of β which maximizes $l(\beta)$, can be obtained by solving the equation $\frac{dl}{d\beta} = 0$ over β. This leads to the following equation (*Page* 1968)

$$\frac{1}{\beta} - \bar{m} + \frac{M_c - M_{max} e^{-\beta(M_{max}-M_c)}}{1 - e^{-\beta(M_{max}-M_c)}} = 0, \qquad \bar{m} = mean\{m | m \in M\}. \tag{5}$$

$\hat{\beta}$ is then the solution of Eq. 5. Now, for each possible M_c, there is an estimated $\hat{\beta}$ and correspondingly an $l(\hat{\beta})$. Then, the optimal M_c will be selected as the one corresponding to the maximum $l(\hat{\beta})$. The standard deviation of the M_c can be calculated using a bootstrap method (see *Shao and Tu* 1995).

The a and b values in Eq. 1 are generally considered as constant in classic frequency-magnitude relation. However, in georeservoirs and in particular during fluid injection, this is not valid. Here, the stress field changes, and thus fracture propagation are obviously time-dependent processes. Therefore, a and b values should also be estimated as time-dependent parameters.

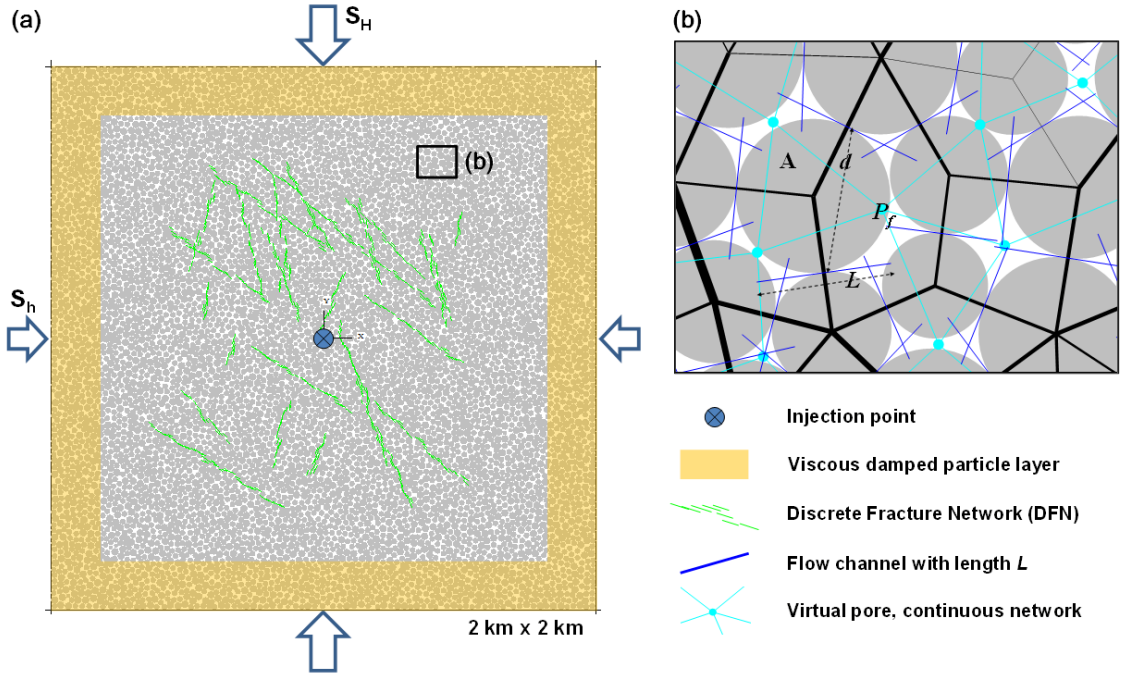

Figure 2. (a) Reservoir model in 2 km × 2 km size with embedded discrete fracture network and subjected to anisotropic in situ stress of S_H = 75 MPa and S_h = 60 MPa. b Close-up view of boxed area showing concept of hydromechanical coupling scheme: discrete particles (*grey*), void spaces filled with interconnected virtual pores.

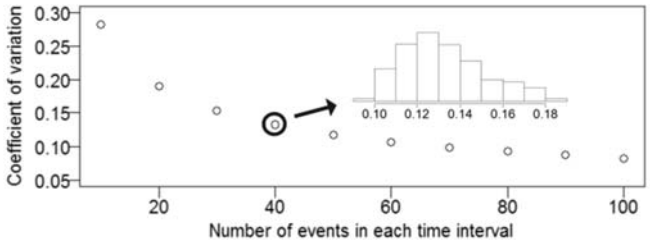

Figure 3. Average coefficient of variations of estimated ***b*** values for different number of events in each time interval calculated using the seismicity catalogue corresponding to the type 1 injection scenario. The histogram shows the distribution of the coefficient of variations corresponding to the case of 40 events.

In order to estimate the time-dependent a value, which is also equivalent to the occurrence rate of events with magnitudes larger than M_c, the time-dependent frequency of events is considered using a bandwidth equal to 0.1 h. The a value uncertainties are calculated due to changes in the catalogue caused by exchanging M_c with M_c +one standard deviation (for the lower uncertainty bound of a value) and M_c −one standard deviation (for the upper uncertainty bound of a value).

The time-dependent b values are estimated using a maximum likelihood estimator for the bounded exponential distribution, i.e. maximizing Eq. 4, of different time intervals (*Page* 1968). We consider overlapping time intervals (see *Nuannin et al.* 2005) that include a constant number of events; selecting this constant number is a trade-off. In general, if the number of events involved in the estimation process increases, the variance of estimated b value decreases (see *Marzocchi and Sandri* 2003). However, the detailed changes of b value will be missing. Therefore, one has to make a compromise between the accuracy and the resolution of the estimated time-dependent b values. To select the optimal number of events in each interval, the average coefficient of variations (the standard deviation divided by the mean value) of estimated b values are observed. Figure 3 shows the average coefficient of variations for different numbers of events in each time interval calculated using the synthetic seismicity catalogue of the commonly used sequential injection type where fluid flow rate is in-creased stepwise.

According to Fig. 3, the point around 40 events is selected, since it locates around the middle of the hyperbolic shape curve with acceptable average coefficient of variations around 0.06. Therefore, the number of events in each time interval is selected equal to 40. The internal histogram in Fig. 3 represents the distribution of the coefficient of variations of estimated b values corresponding to the case of 40 events in each time interval. The histogram shows that the coefficients of variations are convergent around their average. Then, the b value of each time interval is estimated using the magnitudes of events included in the corresponding time interval. The standard deviations of the b values are calculated using a bootstrap method (*Shao and Tu* 1995).

According to Eq. 3, the probability of a magnitude larger than a given magnitude m_g ($M_c \leq m_g \leq M_{max}$) can be calculated by

$$\Pr\left(M \geq m_g \mid M_c \leq m_g \leq M_{max}\right) = 1 - \frac{1 - e^{-\beta(m_g - M_c)}}{1 - e^{-\beta(M_{max} - M_c)}}. \quad (6)$$

The occurrence rate of induced events with magnitudes larger than m_g (e.g. the individual SEECo magnitude in dependence of the local setting and regulatory framework of the corresponding operators) can finally be calculated by

$$\vartheta = \alpha \Pr\left(M \geq m_g \mid M_c \leq M \leq M_{max}\right) \quad (7)$$

Parameters α and β in Eqs. 6 and 7 will then be replaced by time-dependent α_t and $\beta_t \cdot \ln 10$ in order to calculate the time-dependent occurrence rate of SEECo for each catalogue corresponding to each injection type.

5. FISHA application using four different stimulation types

Four different fluid injection types and the resulting induced seismicity are simulated with the hydromechanical-numerical model and analysed with the FISHA workflow in order to estimate the change of occurrence rate of SEECo. Figure 4 represents the induced events from the model and the injection rate at the injection point of the four injection types: (1) sequential injection with high fluid flow rate, (2) sequential injection with moderate fluid flow rate, (3) cyclic injection with increasing fluid flow rate, and (4) cyclic injection with decreasing fluid flow rate. The total volume of the injected fluid for each of these four injection type remains almost the same. The hazard model is applied to the resulting synthetic catalogues of induced seismicity in order to calculate the time-dependent a and b values using the approach explained in the previous section.

In this study, the hazard ϑ is defined as the maximum time-dependent hourly occurrence rate of events with magnitudes ≥ 1.5 (m_g in Eq. 7) during the period of the study, i.e. 30 h after starting the injection. The magnitude threshold m_g is arbitrarily set to 1.5 with respect to the maximum observed magnitude of 1.42 in the synthetic seismicity catalogues. The hazard is then calculated by Eq. 7 for each synthetic catalogue of induced seismicity. M_{max} in Eq. 7 is arbitrarily chosen as M_{max}. However, for

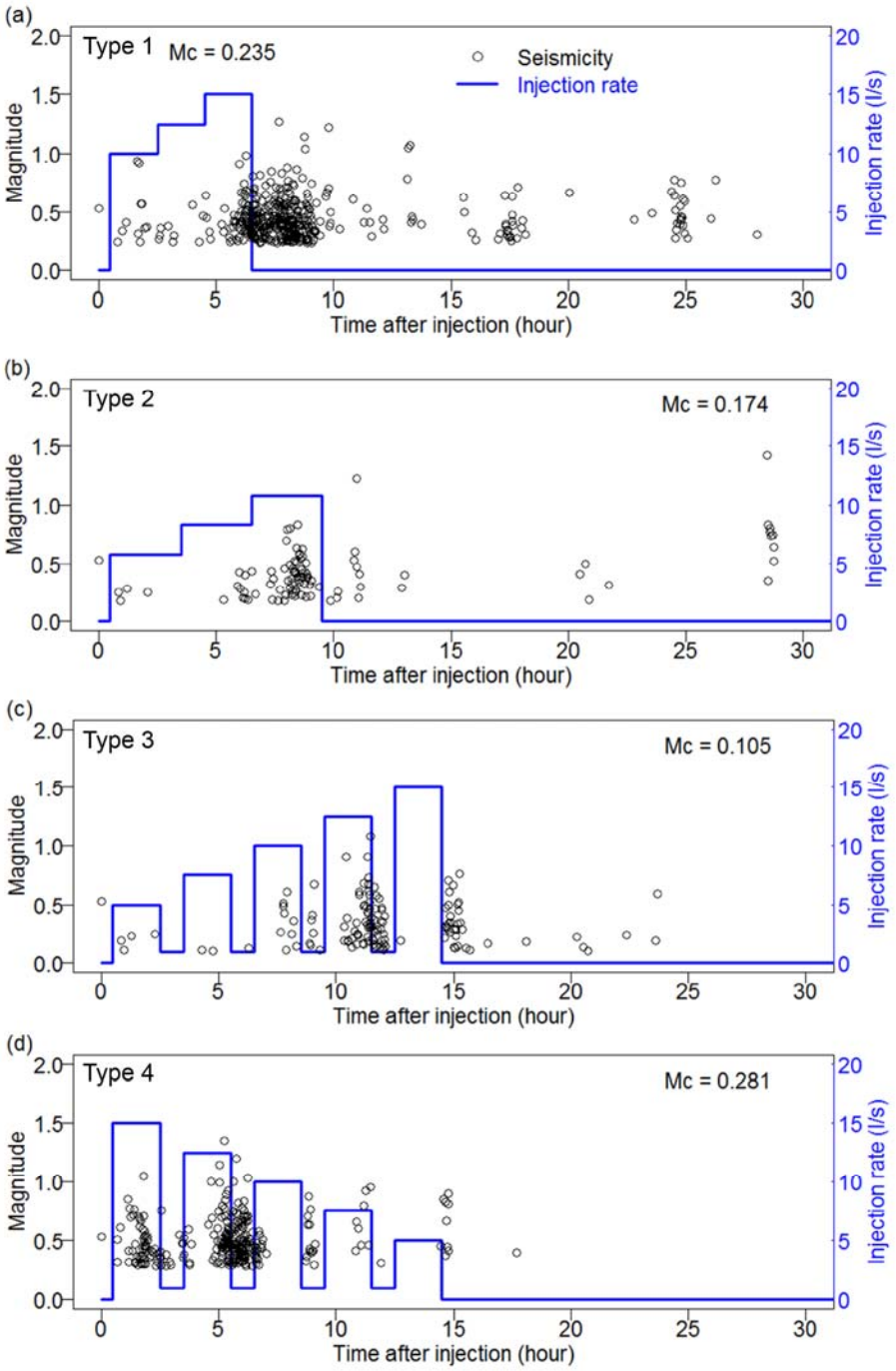

Figure 4. Induced seismicity (*black circles*), fluid injection rate (*blue curves*) and magnitude of completeness M_c. **(a)** Sequential injection with high fluid flow rate. **(b)** Sequential injection with moderate fluid flow rate. **(c)** Cyclic injection with increasing fluid flow rate. **(d)** Cyclic injection with decreasing fluid flow rate.

the real cases of induced seismicity, M_{max} should be estimated. Figure 5 shows the estimated time-dependent a and b values and its standard deviation, as well as the hazard of the four different injection types.

6. Discussion

Table 1 shows the magnitude of completeness M_c (±its standard deviation), the number of events with $M \geq M_c$ (and its upper and lower uncertainty interval due to the standard deviation of M_c), the minimum b value (±its standard deviation) and the hazard ϑ, i.e. the maximum potential hourly occurrence rate of induced events with magnitudes larger than 1.5, corresponding to different injection types. According to Fig. 5a, corresponding to a sequential injection type 1 with high fluid flow rate (Fig. 4a), the hazard ϑ reaches a relatively high value of around 10.15 events/h during 5 to 10 h after the injection. However, in case of Fig. 5b, when the same amount of fluid was injected sequentially into the reservoir, but distributed over a longer period, i.e. with lower fluid flow rate (Fig. 4b), the hazard decreases to 2.59 events/h.

Occurrence of those delayed seismic event clusters in

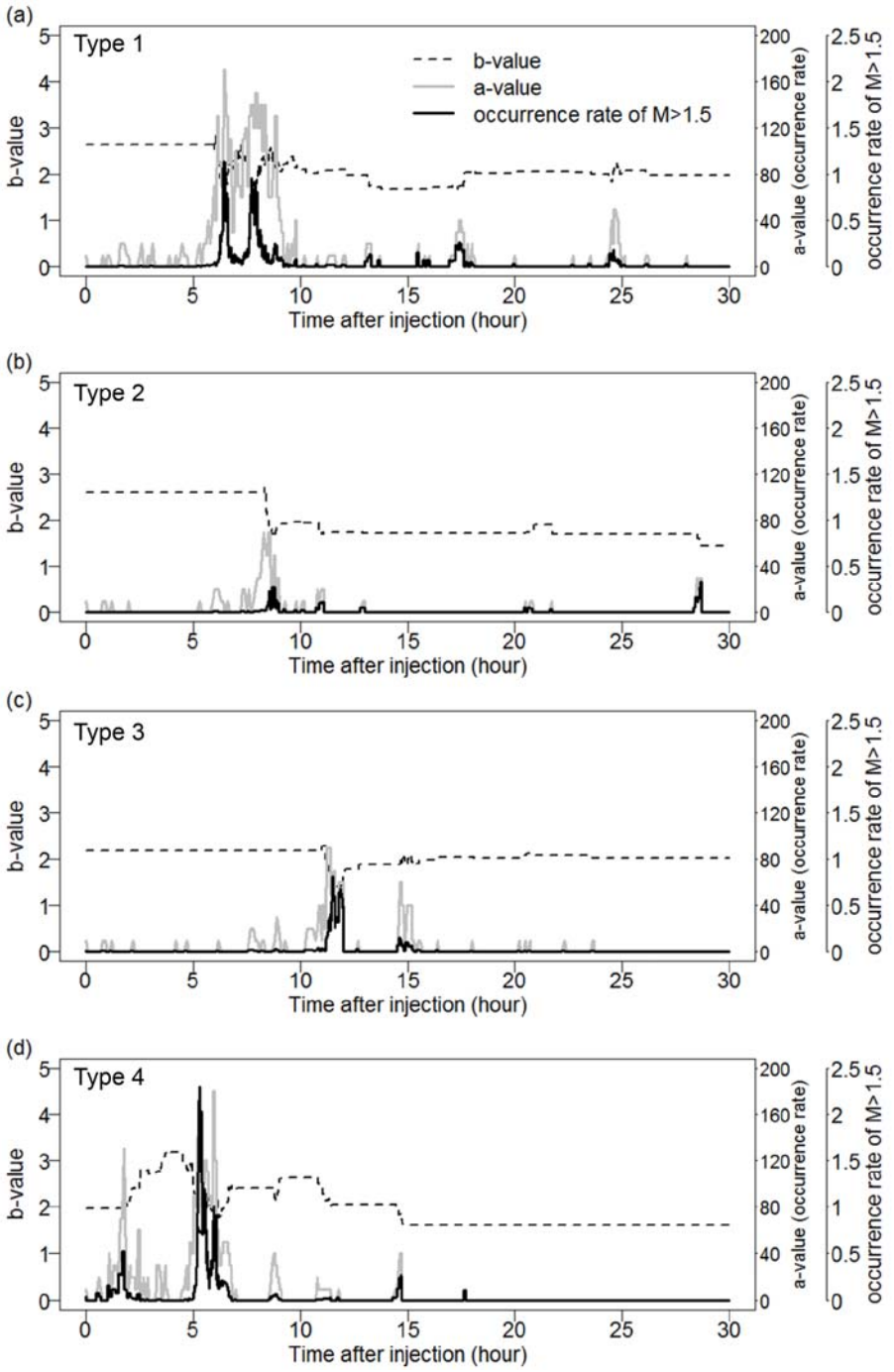

Figure 5. Time-dependent $\boldsymbol{a}$ value and uncertainties due to the standard deviations of $\boldsymbol{M_c}$ (*thick and thin grey curves*), $\boldsymbol{b}$ value ± one standard deviation (*dashed black curves*) and the hazard, i.e. the time-dependent hourly occurrence rate of events with magnitude ≥1.5 (*solid black curves*). **(a)** Sequential injection with high fluid flow rate. **(b)** Sequential injection with moderate fluid flow rate. **(c)** Cyclic injection with increasing fluid flow rate. **(d)** Cyclic injection with decreasing fluid flow rate

the post-shut-in period, first one between 15 and 20 h and second one at ca. 25 h in Fig. 4a, and between 25 and 30 h in Fig. 4b, is due to migration of the pressurized fluid that induces additional seismicity. Such post-shut-in seismicity in a form of relatively dense cluster can be seen in a number of geothermal sites, e.g. Basel 1 EGS (*Häring et al.* 2008).

The hazard corresponding to the cyclic injection with increasing fluid flow rate (type 3, Fig. 4c) yields 1.58 events/h (Fig. 5c), which is lowest corresponding to the hazard. However, the worst case of hazard is obtained from the cyclic injection with decreasing fluid flow rate (type 4, Fig. 4d). In this case, the hazard reaches a value of around 22.06 events/h (Fig. 5d), which is the maximum hazard among all injection types.

From Fig. 5, it is evident that the estimated *a* and *b* values corresponding to different injection types show an opposing trend. While the a value increases, the *b* value starts to decrease and vice versa. In this case, the changes of *a* value are followed by the changes of *b* value. In return, the simultaneous increase in *a* value and decrease in *b* value result in a relatively steep increase in the occur-

Table 1 Magnitude of completeness M_c (±standard deviation), number of events with $M \geq M_c$ (with its uncertainties due to the standard deviations of M_c), minimum b value (±standard deviation) and hazard, i.e. maximum hourly occurrence rate of induced events with magnitude $m_g \geq 1.5$

Injection (type)	M_c	No. of $M \geq M_c$	Min. b value	Hazard
Sequential high flow rate (1)	0.085±0.016	593+[−22, 12]	0.85±0.06	10.15
Sequential moderate flow rate (2)	0.036±0.008	133+[−5, 0]	1.04±0.12	2.59
Cyclic increase of flow rate (3)	0.009±0.003	171+[−3, 0]	1.05±0.09	1.58
Cyclic decrease of flow rate (4)	0.174±0.037	335+[−26, 15]	0.63±0.03	22.06

rence rate of SEECo.

It should be mentioned that the coefficient of variations of the estimated b values for different injection types are relatively high, e.g. the coefficient of variations of minimum b values of different injection types vary between 0.04 and 0.11, (see Table 1). The main reason for that is the relatively lower number of events involving in the estimation of b values in different intervals, i.e. 40 events in each interval (see *Marzocchi and Sandri* 2003). As previously mentioned in "Hazard Model", there is a trade-off between the reliability of the estimated b values and the temporal information in the trend of time-dependent b values. In case of synthetic catalogues, in order to increase the number of generated events, the resolution, in this study the number of particles, of the hydromechanical model should increase. However, the runtime of the model will strongly increase.

Another important issue which should be noted is that the results from the modelling are dependent on the particle size distribution and their arrangement and the bond strength acting on the particle contacts. Some of the bond strength parameters, in particular, tensile and cohesive strengths, are chosen randomly from the given uniform distributions in order to introduce structural and strength heterogeneity in the model. This means that not only the statistical hazard analysis produces uncertainty in the results but also the hydromechanical model itself has intrinsic uncertainty nature, i.e. randomness is involved in structure and properties. It is recommended as a follow-up study to incorporate these model parameter uncertainties to get more general outcomes that are not limited to one specific model geometry and one proper-ties set. This requires many times of simulation runs for each injection scenario on several different models generated by varying the randomness in both structure and properties.

It should be also noted that the presented model and the tested injection scenarios are demonstrative and do not represent any real cases. However, the distribution of the moment magnitude of the numerical seismicity catalogues (which are the key inputs for the FISHA) are in similar ranges com-pared to some field observations, e.g. Soultz GPK2 well stimulation data.

7. Conclusions

We presented the FISHA workflow (Fig. 1) that links the results of hydromechanical-numerical models with time-dependent hazard assessment of induced seismicity. We exemplified FISHA with four reservoir stimulation scenarios using a hydromechanical-numerical model that represents a geothermal reservoir with pre-existing fractures network. This model is capable of generating a catalogue of induced seismic events from the reactivation of pre-existing faults as well as the generation of new fractures, both due to viscous fluid flow through a porous rock mass.

The results of the hazard analysis indicate that injection types 2 and 3, and specially type 3, are generating a significantly lower increase of the occurrence rate of SEECo compared to injection types 1 and 4 (Table 1). Therefore, based on our models, either a cyclic injection with increasing fluid flow rate or a sequential injection with moderate fluid flow rates of longer periods can reduce the occurrence rate of SEECo. From the results, we see that the increase of the a value is accompanied by a decrease in the b value. Therefore, in general, it can be concluded that the hazard follows the a value. This property can be used by EGS field operators allowing first order estimation of the occurrence rate of SEECo by monitoring not only the larger magnitude events, but the occurrence rate of all induced events. This means that when the a value, i.e. the occurrence rate of induced events, starts to steeply increase, the occurrence rate of SEECo steeply increases as well.

The FISHA workflow is general and the hydromechanical-numerical model can be replaced by other models that deliver a synthetic catalogue of induced seismicity or spatiotemporal stress changes. The limiting factor of the reliability of our hazard estimates is the quality of the incorporated geomechanical-numerical model in terms of model parameter uncertainties, boundary and initial conditions as well as model assumptions. Thus, in the next steps, we intend (1) to examine in detail the uncertainties in the FISHA workflow and (2) to apply the approach on other injection strategies.

Acknowledgments The work presented was funded by the European Commission within the FP7 project GEISER, grant agreement no. 241321, by the Department of Energy Geothermal Technologies Program under Award Number DE-EE0002756-002 as well as by Aon Benfield, London. We appreciate the comments from two anonymous reviewers.

References

Altmann J, Müller T, Müller B, Tingay M, Heidbach O (2010) Poroelastic contribution to the reservoir stress path. Int J Rock Mech Min 47(7): 1104–1113

Baisch S, Voros R, Rothert E, Stang H, Jung R, Schellschmidt R (2010) A numerical model for fluid injection induced seismicity at Soultz-sous-Forêts. Int J Rock Mech Min 47(3): 405–413

Barth A, Wenzel F, Langenbruch C (2013) Probability of earthquake occurrence and magnitude estimation in the post shut-in phase of geothermal projects. J Seismol 17(1): 5–11

Bommer JJ, Oates S, Cepeda JM, Lindholm C, Bird J, Torres R, Marroquin G, Rivas J (2006) Control of hazard due to seismicity induced by a hot fractured rock geothermal project. Eng Geol 83: 287–306

Bruel D (2007) Using the migration of induced seismicity as a constraint for fractured hot dry rock reservoir modeling. Int J Rock Mech Min 44: 1106–1117

Cornet FH, Bèrard Th, Bourouis S (2007) How close to failure is a granite rock mass at a 5 km depth? Int J Rock Mech Min 44(1): 47–66

Deichmann N, Ernst J (2009) Earthquake focal mechanisms of the induced seismicity in 2006 and 2007 below Basel (Switzerland). Swiss J Geosci 102: 457–466

Deichmann N, Giardini D (2009) Earthquakes induced by the stimulation of an enhanced geothermal system below Basel (Switzerland). Seismol Res Lett 80(5): 784–798

Dieterich J (1994) A constitutive law for rate of earthquake production and its application to earthquake clustering. J Geophys Res 99(B2): 2601–2618

Dinske C, Shapiro S (2013) Seismotectonic state of reservoirs inferred from magnitude distributions of fluid-induced seismicity. J Seismol 17(1): 13–25

Evans KF, Zappone A, Kraft T, Deichmann N, Moia F (2012) A survey of the induced seismic response to fluid injection in geothermal and CO_2 reservoirs in Europe. Geothermics 41: 30–54

Grünthal G (2013) Induced seismicity related to geothermal projects versus natural tectonic earthquakes and other types of induced seismic events in central Europe. Geothermics. doi: 10.1016/ j.geothermics.2013.09.009

Gutenberg B, Richter CF (1956) Earthquake magnitude, intensity, energy and acceleration (second paper). Bull Seismol Soc Am 46(2): 105–145

Hakimhashemi AH, Schoenball M, Heidbach O, Zang A, Grünthal G (2014) Forward modelling of seismicity rate changes in georeservoirs with a hybrid geomechanical-statistical prototype model. Geothermics. doi: 10.1016/j.geothermics.2014.01.001

Häring MO, Schanz U, Ladner F, Dyer BC (2008) Characterisation of the Basel 1 enhanced geothermal system. Geothermics 37(5): 469–495

Hazzard JF, Young RP (2002) Moment tensors and micromechanical models. Tectonophysics 356: 181–197

Hazzard JF, Young RP (2004) Dynamic modelling of induced seismicity. Int J Rock Mech Min 41(8): 1365–1376

Hubbert MK, Willis DG (1957) Mechanics of hydraulic fracturing. Trans AIME 210: 153–166

Kohl T, Megel T (2007) Predictive modeling of reservoir response to hydraulic stimulations at the European EGS site Soultz-sous-Forets. Int J Rock Mech Min 44(8): 1118–1131

Labuz JF, Zang A (2012) Mohr-Coulomb failure criterion. Rock Mech Rock Eng 45: 975–979

Majer EL, Baria R, Stark M, Oates S, Bommer J, Smith B, Asanuma H (2007) Induced seismicity associated with enhanced geothermal systems. Geothermics 36: 185–222

Majer E, Nelson J, Robertson-Tait A, Savy J, Wong I (2012) Protocol for addressing induced seismicity associated with enhanced geothermal systems. U.S. Department of Energy, DOE/EE-0662

Marzocchi W, Sandri L (2003) A review and new insights on the estimation of the b-value and its uncertainty. Annals of Geophysics 46(6): 1271–1282

McClure MW, Horne HN (2011) Investigation of injection-induced seismicity using a coupled fluid flow and rate and state friction model. Geophysics 76(6): WC183–WC200

Nuannin P, Kulhanek O, Persson L (2005) Spatial and temporal b value anomalies preceding the devastating off coast of NW Sumatra earthquake of December 26, 2004. Geophys Res Lett 32: (L11307)

Page R (1968) Aftershocks and microaftershocks of the Great Alaska earthquake of 1964. Bull Seismol Soc Am 58(3): 1131–1168

Rutqvist J, Birkholzer J, Cappa F, Tsang C-F (2007) Estimating maximum sustainable injection pressure during geological sequestration of co2 using coupled fluid flow and geomechanical fault-slip analysis. Energy Conversion and Management 48: 1798–1807

Schoenball M, Müller TM, Müller B, Heidbach O (2010) Fluid-induced microseismicity in pre-stressed rock masses. Geophys J Int 180: 113–119

Shao J, Tu D (1995) The jackknife and bootstrap. Springer Series in Statistics

Shapiro S, Dinske C, Langenbruch C, Wenzel F (2010) Seismogenic index and magnitude probability of earthquakes induced during reservoir fluid stimulations. Leading Edge 29(3): 304–309

Stigler SM (2007) The epic story of maximum likelihood. Statistical Science 22(4): 598–620

Suckale J (2009) Induced seismicity in hydrocarbon fields. Adv Geophys 51: 55–106

Suckale J (2010) Moderate-to-large seismicity induced hydrocarbon production. The Leading Edge 310–317

Yoon JS, Zang A, Stephansson O (2013) Simulation of hydraulic stimulation of fractured reservoir and induced seismicity using discrete element-fracture network model. Proceedings of Thirty-Eighth Workshop on Geothermal Reservoir Engineering, Stanford University, Stanford, California, February 11–13, 2013, SGP-TR-198

Yoon JS, Zang A, Stephansson O (2014) Numerical investigation of optimized stimulation of intact and naturally fracture deep geothermal reservoirs using hydro-mechanical coupled discrete particles joints model. Geothermics. doi: 10.1016/j.geothermics.2014.01.009

Zang A, Yoon JS, Stephansson O, Heidbach O (2013) Fatigue hydraulic fracturing by cyclic reservoir treatment enhances permeability and reduces induced seismicity. Geophys J Int 195: 1282–1287